IAC-14-A7.2.6

MICRO-SPEC: AN INTEGRATED, DIRECT-DETECTION SPECTROMETER FOR FAR-INFRARED AND SUBMILLIMETER ASTRONOMY

Giuseppe Cataldo

NASA Goddard Space Flight Center, United States of America, Giuseppe.Cataldo@NASA.gov

Massachusetts Institute of Technology, United States of America, gcataldo@mit.edu

The far-infrared and submillimeter portions of the electromagnetic spectrum provide a unique view of the astrophysical processes present in the early universe. Our ability to fully explore this rich spectral region has been limited, however, by the size and cost of the cryogenic spectrometers required to carry out such measurements. Micro-Spec (μ-Spec) is a high-sensitivity, direct-detection spectrometer concept working in the 450–1000 μm wavelength range which will enable a wide range of flight missions that would otherwise be challenging due to the large size of current instruments with the required spectral resolution and sensitivity. The spectrometer design utilizes two internal antenna arrays, one for transmitting and one for receiving, superconducting microstrip transmission lines for power division and phase delay, and an array of microwave kinetic inductance detectors (MKIDs) to achieve these goals. The instrument will be integrated on a ~ 10 cm^2 silicon chip and can therefore become an important capability under the low background conditions accessible via space and high-altitude borne platforms. In this paper, an optical design methodology for μ-Spec is presented, with particular attention given to its two-dimensional diffractive region, where the light of different wavelengths is focused on the different detectors. The method is based on the maximization of the instrument resolving power and minimization of the RMS phase error on the instrument focal plane. This two-step optimization can generate geometrical configurations given specific requirements on spectrometer size, operating spectral range and performance. A point design with resolving power of 257, an RMS phase error less than 0.1 radians and four stigmatic points was developed for initial demonstration and will be the basis of future instruments with resolving power up to about 1200.

I. INTRODUCTION

Far-infrared (IR) and submillimeter (15 μm–1 mm) spectroscopy provides a powerful tool to probe a wide range of environments in the universe. In the past thirty years, discoveries made by several space-based observatories have provided unique insights into physical processes leading to the evolution of the universe and its contents. This information is encoded in a wide range of molecular lines and fine structure lines. Observations of such spectral lines enable the exploration of galaxies at high redshifts. The fine structure lines of abundant elements (C, N and O) allow tracing the obscured star formation and AGN activity into the high-redshift universe. One can measure galaxy redshifts and determine their elemental abundances and physical conditions out to redshifts of $z > 5$. In spite of this, a number of questions remain unanswered regarding the very early steps of the universe as well as galactic, stellar and planetary formation. The ability to fully explore this rich spectral region has been limited by the size and cost of the cryogenic spectrometers required to carry out these measurements. The work proposed here specifically addresses the need for integrated spectrometers and ultra-low-noise, far-IR, direct detectors, whose specific requirements are shown in Table 1 and compared against the current state of the art.

To contribute to realizing the goals outlined in Table 1

Metric	State of the art	Requirements
Wavelength, λ	$250 - 700$ μm	$220 - 2000$ μm
Sensitivity, NEP	10^{-19} W/$\sqrt{\text{Hz}}$	10^{-21} W/$\sqrt{\text{Hz}}$
Resolution, $\mathcal{R}$	≥ 100	≥ 1200
Detective quantum efficiency, DQE	$\sim 15\%$	$> 90\%$
Temperature, T	< 1 K	~ 0.05 K
Time constant, τ	100 ms	< 10 ms

Table 1: Summary of far-IR spectrometer and detector array requirements and comparison with current state of the art [1].

and fill in the gaps in the current state of the art, a high-performance integrated spectrometer module, Micro-Spec (μ-Spec), operating in the 450–1000 μm (300–650 GHz) range is proposed. With μ-Spec (Fig. 1), the incoming radiation collected by the telescope is coupled to the spectrometer via a broadband dual-slot antenna used in conjunction with a hyper-hemispeherical silicon lens and directed to a series of power splitters and a delay network made of superconducting microstrip transmission lines. The delay network creates a retardation across the input to a planar waveguide multimode region, which has two internal antenna arrays, one for transmitting and one for receiving the radiation as a function of wavelength. Absorber structures lining the multimode region
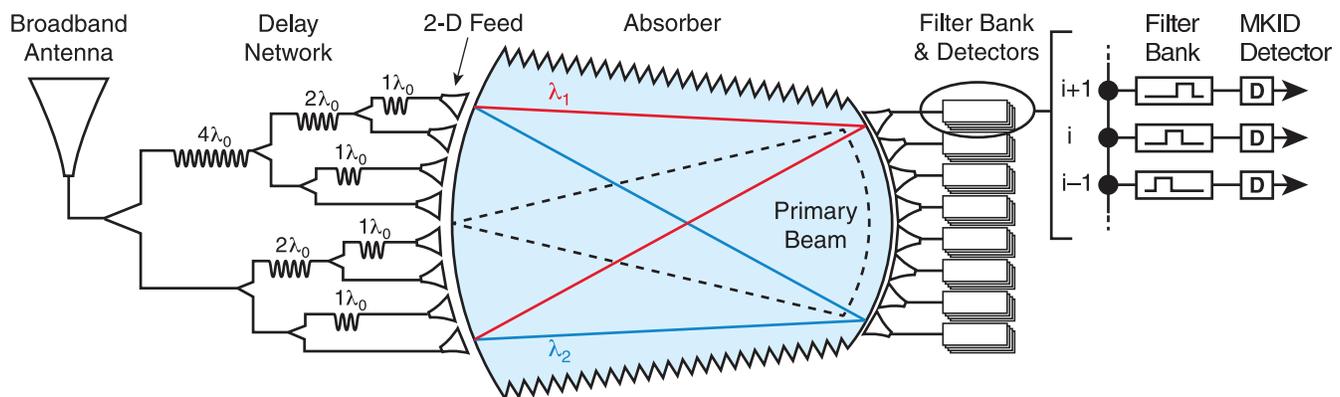
Figure 1: Layout of the μ-Spec module. The radiation is coupled into the instrument through a broadband antenna and is then transmitted through a superconducting transmission line to a divider and a phase delay network. The spectrum enters the multimode region through an array of feeds which concentrates the power along the focal surface with different wavelengths at different locations. The receivers are connected to a bank of order-sorting filters and MKID detectors [2].

control the power emitted into large angles or reflected from the receiver antenna array. An array of feed structures is employed to couple the radiation to the multimode region and concentrates the power along the focal surface with different wavelengths at different locations. The outputs are connected to a bank of order-sorting filters which terminate the power in an array of microwave kinetic inductance detectors (MKIDs) for detection and readout. The entire instrument is integrated on a 100-mm-diameter silicon chip. This size in reduction is accomplished through the use of single-mode microstrip delay lines, which can compactly be folded on the silicon wafer and reduce the required physical line length by a factor of the medium's effective refractive index.

The frequency range of the implementation presented here is limited to wavelengths $\lambda > 250$ μm by the gap frequency of currently available low-loss superconductors. These include niobium (Nb) and niobium-titanium nitride (NbTiN) for the transmission line structures, and molybdenum nitride (MoN) for the detectors.

Finally, μ-Spec can be compared to a grating spectrometer [3], in which a plane wave is reflected from the grating and the phase of each partial wave scattered from the rulings is a linear function of position across the grating. However, it differs from similar technologies by the order of processing of the light in the spectrometer. For instance, in a Rowland spectrometer the required phase retardation is generated by reflection from the grating grooves [3, 4, 5, 6, 7], whereas in Z-Spec, which is an example of planar Rowland grating architecture, propagation occurs in parallel-plate waveguides [8, 9, 10, 11]. A last comparison can be made with one-dimensional bootlace lenses found in microwave practice [12, 13, 14, 15], which μ-Spec builds upon for submillimeter wave applications. This paper will describe the design process of the multimode region and illustrate the results in terms of geometry, imaging quality and efficiency.

II.   MULTIMODE REGION DESIGN

A prototype version with a resolving power $\mathcal{R} = 65$ in first order was designed [2] and built, and is currently under evaluation at the NASA Goddard Space Flight Center. This design was specified by requiring the phase error to vanish at three specific stigmatic points on the focal plane. This can be seen as a generalization of the approach described in [8] with two stigmatic points. In [16], designs were presented for $\mathcal{R} = 260$ and $\mathcal{R} = 520$ in higher order and with zero phase error imposed on three preselected stigmatic points. These designs were obtained through a constrained, non-linear optimization process. A fourth stigmatic point was observed beyond the angular range in use. It is the purpose of this work to show how to use this additional degree of freedom to increase the number of spectrometer channels and resolving power. In the following section, therefore, we describe a design for $\mathcal{R} = 260$ in first order with zero phase error at all four stigmatic points, as a result of an unconstrained optimization process which maximizes the instrument performance.

II.I.   Problem formulation

As explained in [2], the design variables are the x and y coordinates of the N_e emitters' centers and the electrical path lengths in silicon, R_i^e, for each feed's electrical delay. The resolving power is defined as

$$\mathcal{R} = M \cdot N_e, \tag{1}$$

where M is the order of the spectrometer and N_e is some power of 2, given the structure of the power divider network (see Fig. 1). The first step of the design consists of finding the maximum achievable resolving power, $\mathcal{R}_{max}$, as a function of M and the relative emitter pitch, $\eta = p/\lambda_{avg}$ ($p =$ emitter pitch, $\lambda_{avg} =$ central wavelength associated with the geometric average frequency - see Fig. 2), given specific re-

quirements on spectrometer radius, R, and operating spectral range as well as certain constraints on performance.
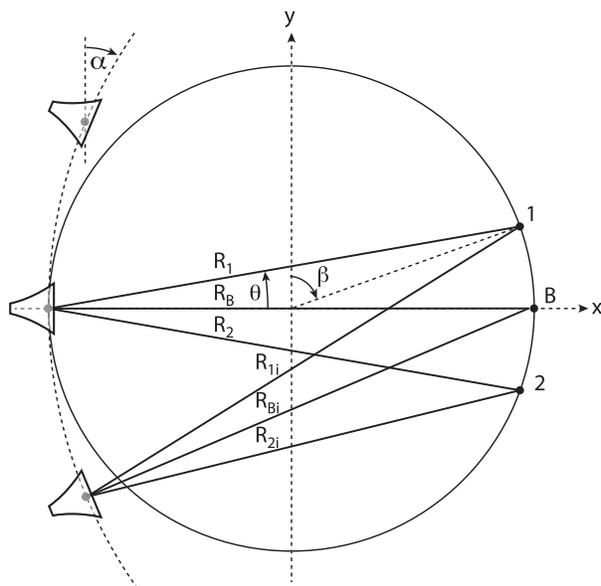

Figure 2: Simplified representation of the grating geometry. On the left side three radiators can be seen, which point to the blaze point, B. The path from each radiator's phase center to the first and second stigmatic points are also indicated by solid lines for the array's i-th and central reference feed [2].

The formulation of this mixed integer non-linear problem is as follows:

$$\max \mathcal{R}_{max}(M, \eta) = M/\eta \cdot R/\lambda_{avg} \quad (2)$$
$$\text{subject to} \quad H_e(M, \eta) \leq R \quad (3)$$
$$H_r(M, \eta) \leq \pi R \quad (4)$$
$$\mathcal{R}_{max}(M, \eta) > 200 \quad (5)$$
$$\eta > 0 \quad (6)$$
$$M \geq 1, \quad M \text{ integer} \quad (7)$$

Equation (3) imposes that the width of the emitter array, H_e, be less than or equal to the radius so that there is no aberration; eq. (4) lets the receiver array be as large as the focal plane to optimize its utilization; and constraint (5) sets a minimum value for the required maximum resolving power, thereby eliminating solutions in which we are not interested. Finally we note that, to enlarge the tradespace, the constraint of equal emitter and receiver pitch, used in our previous designs, was removed.

Table 2 shows the requirements on spectrometer size and spectral range used for this problem. The minimum and maximum frequencies are no longer associated with any stigmatic point and fall within the spectral range defined in Table 1. The average frequency was computed as their geometric mean. The objective spaces as a function of M and η are shown in Fig. 3. On the left (Fig. 3a), it is possible to visualize the feasible objective space of the optimization problem described above for $\mathcal{R}_{max}$ along with the active constraint, Eq. (4) (blue area). The feasible solutions to Problem (2) populate that part of the contour plot above the blue area, whereas the optimal solutions lie at the intersection of the active constraint with the largest $\mathcal{R}_{max} \sim 275$, one for each value of M. We decided to investigate the first-order case as an example of simple and robust system. Higher-resolution instruments will certainly require higher-order operations. Table 3 shows the values of the design variables associated with this particular optimal solution as well as the values of the constraints (3)-(7), which are all satisfied.

Once this problem solved, it was then possible to compute the number of emitters, $N_e = \mathcal{R}_{max}/M$, and round it down to a power of 2. According to Eq. (1), this causes the actual resolving power, $\mathcal{R}$, calculated with this updated value of N_e, to be lower than $\mathcal{R}_{max}$. The plot in Fig. 3b shows the values of $\mathcal{R}$ (red line) and the values of M and η that would make such realizations possible. For $M = 1$, $\mathcal{R} = 257$.

Parameter	Symbol	Unit	Value
Multimode region radius	R	cm	1.25
Minimum frequency	f_{min}	GHz	430.0
Maximum frequency	f_{max}	GHz	650.0
Average frequency	f_{avg}	GHz	528.7

Table 2: Requirements on spectrometer size and spectral range

| Variable	Symbol	Unit	Value
Spectrometer order	M	-	1
Relative emitter diameter	η	-	0.2916
Maximum resolving power	$\mathcal{R}_{max}$	-	275
Emitter array width	H_e	cm	1.2452
Receiver array width	H_r	cm	3.5674
Emitter pitch	p	cm	0.0048
Receiver pitch	s	cm	0.0167
Number of emitters	N_e	-	257
Number of receivers	N_r	-	149
Resolving power	$\mathcal{R}$	-	**257**

Table 3: Optimal solution to Problem (2) for $M = 1$

The second step toward determining the optimal solution in terms of the above-mentioned design variables consists in minimizing the overall RMS phase error, φ_{RMS}, through a figure of merit representing the area subtended by φ_{RMS} on the focal plane:

$$\min \int_0^\pi \varphi_{\text{RMS}} \, \mathrm{d}\theta, \quad (8)$$

IAC-14-A7.2.6
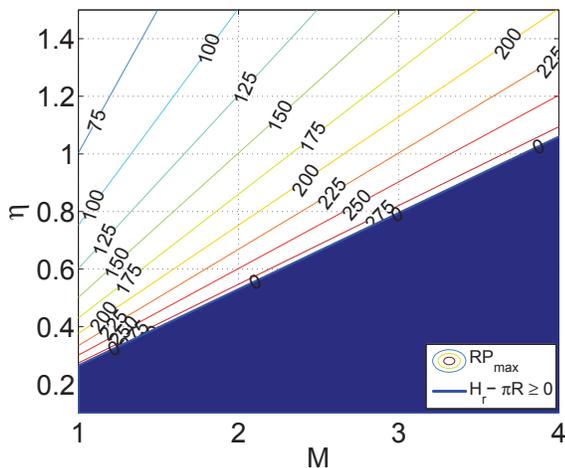
(a) The contour plot depicts all the feasible values of $\mathcal{R}_{max}$ and shows that for each M a solution exists that satisfies all constraints.
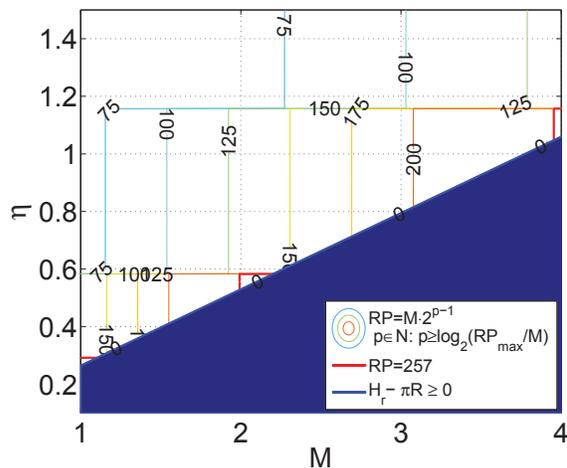
(b) The contour plot represents the feasible values of $\mathcal{R}$ for all orders given as powers of 2. The $\mathcal{R} = 257$ red curve identifies the optimal solution.

Figure 3: Objective spaces of Problem (2). The blue area represents the infeasible region which, in this case, coincides with the active constraint in Eq. (4).

with

$$\varphi_{\mathrm{RMS}} = \sqrt{\sum_{i=1}^{N_e} \frac{[\varphi_{ij}(x_i, y_i, \tau_i, \theta_j) - \langle\varphi(\theta_j)\rangle]^2}{N_e}}. \qquad (9)$$

Here, φ_{ij} is the relative phase of each transmitter, $\langle\varphi(\theta_j)\rangle = 0$ is the relative phase of the central transmitter (this is zero by construction as the central radiator is used as a reference) and θ_j represents the angle corresponding to each of the points in which the focal plane was discretized. When setting Eq. (9) equal to zero, its analytical expression is a fourth-order function of the focal plane angle, θ, which implies that at most four stigmatic points can be obtained. By solving problem (8) over the entire focal plane, i.e., $0 \leq \theta \leq \pi$, one could in principle find these four solutions, provided they are not degenerate.

II.II. Optimization results

The solution to the minimization problem defined in Eq. (8) can be seen in Fig. 4. The emitters' positions are indicated in red and present several characteristics similar to those found and discussed in [16]. First, they do not lie on the grating circle but on a curve that is tilted leftwards and intersects the grating circle at the central emitter before ending up inside the multimode region. It was verified that the shape of this curve only approximates a circle with a radius $\sim 2.2R$ and is not symmetric. In the case presented here, this is caused by the absence of constraints on all stigmatic points. In general, for a two-stigmatic-point configuration the emitters lie exactly on the grating circle, as shown in the literature [3, 8]. The imposition of zero RMS phase error on a third stigmatic point (the blaze point) also caused a similar tilting effect [16],

unless the emitters could be constrained to lie within a small distance (e.g., $\lambda_1/8$) from the $2R$ circle, as shown in our previous work [2].
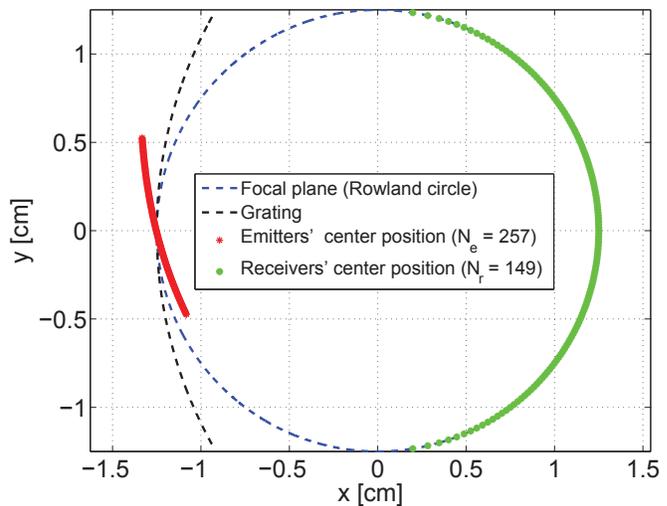

Figure 4: Optimized multimode region design with a resolving power $\mathcal{R} = 257$ and order $M = 1$.

The RMS phase error is shown in Fig. 5. Its values remain below 0.1 radians over an angular range spanning from approximately $16°$ to $176°$. This represents a $\sim 30\%$ improvement in the focal plane utilization over the previous designs [2, 16]. Four stigmatic points are visible, but it is important to note that they are no longer associated with a predefined frequency, given the absence of constraints on them.

In Fig. 5 it can be seen to what frequencies they correspond in this design. The nominal spectral range indicated in Table 2 is only partially covered down to ~ 510 GHz at $0°$, while above $130°$ frequencies higher than 650 GHz show up, where niobium is no longer a superconductor. To ensure that the entire nominal spectral range be used on the focal plane, future efforts will be focused on solving Eq. (8) with constraints on all four stigmatic points and to iteratively adjust the lower bound of the nominal spectral range in the attempt to look for alternative designs satisfying these requirements. Finally, while our previous designs present an RMS phase error smaller than 0.005 radians, a maximum value of 0.1 for this quantity is still representative of high-quality spectrometers.
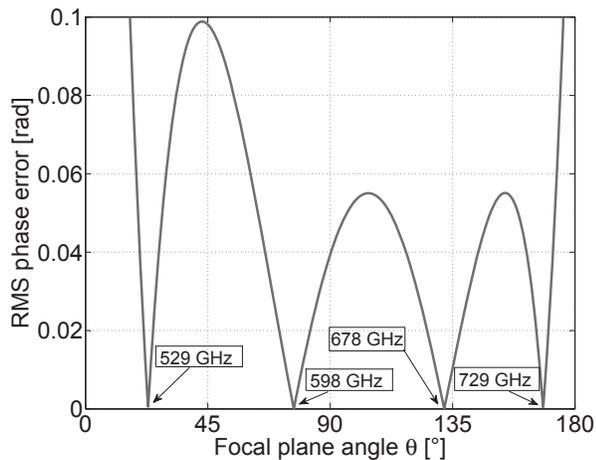

Figure 6: Comparison of the efficiency of the design presented in this paper and the ones from [2, 16].

Figure 5: RMS phase error. The worst value is 0.1 radians at almost $45°$ and four stigmatic points can be seen over a $160°$ angular range.

II.III.   Power efficiency

The power coupling in the new design configuration was computed with the model described in [2], Sec. 4. The ratio of the power emitted by the feed horns to the power received by the antennas is equal to 1. This high efficiency is the result of the absence of any higher-order diffraction peaks in the multimode region due to the relative emitter diameter, η, being smaller than 1/2, as required to avoid diffraction [17]. Figure 6 illustrates the values of the normalized power for the $\mathcal{R} = 257$ configuration discussed in this work as well as for all our previous designs [2, 16]. The current configuration outperforms all those in first order in terms of efficiency, while simultaneously providing a medium-high resolution.

III.   CONCLUSIONS

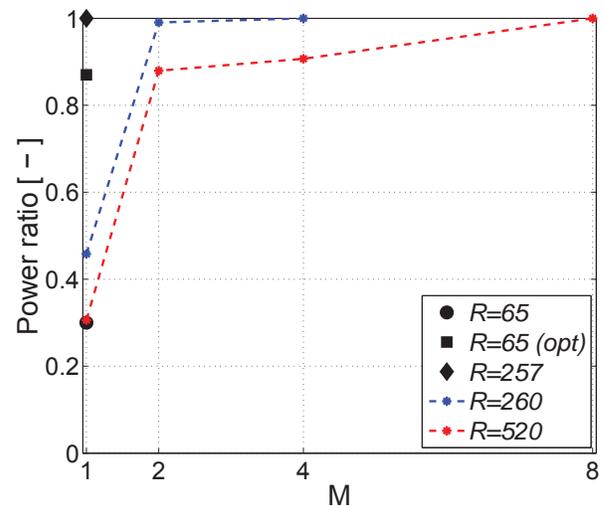A design methodology has been developed for high-resolution configurations of the μ-Spec multimode region. The design procedure first maximizes the resolving power subject to constraints on geometry, operating frequency range and performance, thereby determining the order of the spectrometer. This then allows the RMS phase error on the instrument focal plane to be minimized. This work discussed a particular design achieved without constraining the RMS phase error to vanish at preselected stigmatic points on the focal plane. This led to a configuration with four stigmatic points spread over nearly the entire focal plane, a feature which can be used to increase the number of spectrometer channels. This design achieves a maximum RMS phase error equal to 0.1 radians and a resolution of 257 in first order. Due to the complete lack of diffraction, it presents a coupling efficiency of 1. Future work will be aimed at employing this design methodology to generate higher-resolution ($\mathcal{R} > 500$) configurations with maximum utilization of the focal plane and RMS phase error less than 0.1.

References

[1] R. D. Barney, J. J. Bauman, L. D. Feinberg, D. J. Mccleese, U. N. Singh, and H. P. Stahl. NASA's Space Technology Roadmap - Science Instruments, Observa-

tories, and Sensor System Roadmap, Technology Area 08. Technical report, NASA, 2012.

[2] G. Cataldo, W.-T. Hsieh, W.-C. Huang, S. H. Moseley, T. R. Stevenson, and E. J. Wollack. Micro-Spec: an ultracompact, high-sensitivity spectrometer for far-infrared and submillimeter astronomy. *Applied Optics*, 53:1094–1102, 2014.

[3] H. A. Rowland. On concave gratings for optical purposes. *Philosophical Magazine*, 16:197–210, 1883.

[4] H. W. Yen, H. R. Friedrich, R. J. Morrison, and G. L. Tangonan. Planar Rowland spectrometer for fiber-optic wavelength demultiplexing. *Optics Letters*, 6 (12):639–641, 1981.

[5] R. März and C. Cremer. On the Theory of Planar Spectrograph. *Journal of Lightwave Technology*, 10:2017–2022, 1992.

[6] M. Wu and Y. J. Chen. Design Considerations for Rowland Circle Gratings Used in Photonic Integrated Devices for WDM Applications. *Journal of Lightwave Technology*, 12 (11):1939–1942, 1994.

[7] P. Muñoz, D. Pastor, J. Capmany, and A. Martínez. Geometrical optimization of the transmission and dispersion properties of arrayed waveguide gratings using two stigmatic point mountings. *Optics Express*, 11:2425–2432, 2003.

[8] B. J. Naylor. *Broadband Millimeter-Wave Spectroscopy with Z-Spec: An Unbiased Molecular-Line Survey of the Starburst Galaxy M82*. PhD thesis, California Institute of Technology, 2008.

[9] C. M. Bradford, B. J. Naylor, J. Zmuidzinas, J. J. Bock, J. Gromke, H. Nguyen, M. Dragovan, M. Yun, L. Earle, J. Glenn, H. Matsuhara, P. A. R. Ade, and L. Duband. WaFIRS, a waveguide far-IR spectrometer: enabling spectroscopy of high-z galaxies in the far-IR and submillimeter. In *Space Telescopes and Instruments*, volume 4850 of *Society of Photo-Optical Instrumentation Engineers (SPIE)*, pages 1137–1147, 2003.

[10] C. M. Bradford, P. A. R. Ade, J. Aguirre, J. J. Bock, L. Duband, L. Earle, J. Glenn, H. Matsuhara, B. J. Naylor, H. Nguyen, M. Yun, and J. Zmuidzinas. Z-Spec: a broadband millimeter-wave grating spectrometer - design, construction, and first cryogenic measurements. In *Millimeter and Submillimeter Detectors for Astronomy II*, volume 5408 of *Society of Photo-Optical Instrumentation Engineers (SPIE)*, pages 257–267, 2004.

[11] L. Earle, P. A. R. Ade, J. Aguirre, R. Aikin, J. Battle, J. J. Bock, C. M. Bradford, M. Dragovan, L. Duband, J. Glenn, G. Griffin, V. Hridtov, P. Maloney, H. Matsuhara, B. J. Naylor, H. Nguyen, M. Yun, and J. Zmuidzinas. Z-Spec: a broadband, direct-detection, millimeter-wave spectrometer - instrument status and first results. In *Millimeter and Submillimeter Detectors for Astronomy III*, volume 6275 of *Society of Photo-Optical Instrumentation Engineers (SPIE)*, pages 1–9, 2006.

[12] W. Rotman and R. F. Turner. Wide-Angle Microwave Lens for Line Source Applications. *IEEE Transactions on Antennas and Propagation*, 11 (6):623–632, 1963.

[13] T. Katagi, S. Mano, and S. I. Sato. An improved design method of Rotman lens antennas. *IEEE Transactions on Antennas and Propagation*, 32 (5):524–527, 1984.

[14] R. C. Hansen. Design trades for Rotman lenses. *IEEE Transactions on Antennas and Propagation*, 39 (4):464–472, 1991.

[15] C. M. Rappaport and A. I. Zaghloul. Multifocal Bootlace Lens Design Concepts: a Review. In *IEEE Antennas and Propagation Society International Symposium*, volume 2B of *Institute of Electrical and Electronics Engineers (IEEE)*, pages 39–42, 2005.

[16] G. Cataldo, W.-T. Hsieh, W.-C. Huang, S. H. Moseley, T. R. Stevenson, and E. J. Wollack. Micro-Spec: an integrated direct-detection spectrometer for far-infrared space telescopes. In *Space Telescopes and Instrumentation 2014: Optical, Infrared, and Millimeter Wave*, volume 9143 of *Society of Photo-Optical Instrumentation Engineers (SPIE)*, pages 91432C–91432C–9, 2014.

[17] R. C. Hansen. *Phased Array Antennas*. Wiley, 1998.